Integrity of the Cone Photoreceptor Mosaic in Oligocone Trichromacy

Michel Michaelides,[1,2,3] *Jungtae Rha,*[3,4] *Elise W. Dees,*[5] *Rigmor C. Baraas,*[5] *Melissa L. Wagner-Schuman,*[6] *John D. Mollon,*[7] *Adam M. Dubis,*[8] *Mette K. G. Andersen,*[9,10] *Thomas Rosenberg,*[9] *Michael Larsen,*[9,10] *Anthony T. Moore,*[1,2] *and Joseph Carroll*[4,6,8]

Purpose. Oligocone trichromacy (OT) is an unusual cone dysfunction syndrome characterized by reduced visual acuity, mild photophobia, reduced amplitude of the cone electroretinogram with normal rod responses, normal fundus appearance, and normal or near-normal color vision. It has been proposed that these patients have a reduced number of normal functioning cones (oligocone). This paper has sought to evaluate the integrity of the cone photoreceptor mosaic in four patients previously described as having OT.

Methods. Retinal images were obtained from two brothers (13 and 15 years) and two unrelated subjects, one male (47 years) and one female (24 years). High-resolution images of the cone mosaic were obtained using high-speed adaptive optics (AO) fundus cameras. Visible structures were analyzed for density using custom software. Additional retinal images were obtained using spectral domain optical coherence tomography (SD-OCT), and the four layers of the photoreceptor-retinal pigment epithelium complex (ELM, IS/OS, RPE1, RPE2) were evaluated. Cone photoreceptor length and the thickness of intraretinal layers were measured and compared to previously published normative data.

Results. The adult male subject had infantile onset nystagmus while the three other patients did not. In the adult male patient, a normal appearing cone mosaic was observed. However, the three other subjects had a sparse mosaic of cones remaining at the fovea, with no structure visible outside the central fovea. On SD-OCT, the adult male subject had a very shallow foveal pit, with all major retinal layers being visible, and both inner segment (IS) and outer segment (OS) length were within normal limits. In the other three patients, while all four layers were visible in the central fovea and IS length was within normal limits, the OS length was significantly decreased. Peripherally the IS/OS layer decreased in intensity, and the RPE1 layer was no longer discernable, in keeping with the lack of cone structure observed on AO imaging outside the central fovea.

Conclusions. Findings are consistent with the visual deficits being caused by a reduced number of healthy cones in the two brothers and the adult female. In the unrelated adult subject, no structural basis for the disorder was found. These data suggest two distinct groups on the basis of structural imaging. It is proposed that the former group with evidence of a reduction in cone numbers is more in keeping with typical OT, with the latter group representing an OT-like phenotype. These two groups may be difficult to readily discern on the basis of phenotypic features alone, and high-resolution imaging may be an effective way to distinguish between these phenotypes. (*Invest Ophthalmol Vis Sci.* 2011;52:4757–4764) DOI: 10.1167/iovs.10-6659

The cone dysfunction syndromes are a heterogeneous group of disorders characterized by an early-onset reduction in central vision associated with a variable degree of photophobia and nystagmus, normal fundus examination, and reduced or absent cone responses with normal rod function on electroretinography.[1] As expected, the abnormal cone function observed in these conditions results in markedly reduced or absent color discrimination, with the degree and pattern of color loss being helpful in differentiating between these disorders.[1] In contrast, oligocone trichromacy (OT) is an unusual cone dysfunction syndrome, characterized by normal or near-normal color vision despite an absent or reduced cone electroretinogram.[1–9]

It has been proposed that these patients have a reduced number of normal functioning cones (oligocone), with preservation of three spectrally distinct types of cone permitting

From the [1]UCL Institute of Ophthalmology, London, United Kingdom; [2]Moorfields Eye Hospital, London, United Kingdom; Departments of [4]Ophthalmology, [6]Biophysics, and [8]Cell Biology, Neurobiology, & Anatomy, Medical College of Wisconsin, Milwaukee, Wisconsin; [5]Department of Optometry and Visual Science, Buskerud University College, Kongsberg, Norway; [7]Department of Experimental Psychology, University of Cambridge, Cambridge, United Kingdom; [9]Gordon Norrie Centre, National Eye Clinic, Glostrup, Denmark; and [10]Department of Ophthalmology, University of Copenhagen, Glostrup Hospital, Copenhagen, Denmark.

[3]Authors contributed equally to this study and therefore should be considered equivalent authors.

Supported by grants from the NIH (EY001931, EY017607, EY014537), Juvenile Diabetes Research Foundation (8-2002-130), the E. Matilda Ziegler Foundation for the Blind, Hope for Vision, an unrestricted grant from Research to Prevent Blindness, Foundation Fighting Blindness (USA), Moorfields Special Trustees, the Guide Dogs for the Blind Association, the National Institute for Health Research UK to the Biomedical Research Centre for Ophthalmology based at Moorfields Eye Hospital, NHS Foundation Trust, and UCL Institute of Ophthalmology, and the Research Council of Norway (182768/V1 & 183789). JC is the recipient of a Career Development Award from Research to Prevent Blindness. This investigation was conducted in facilities constructed with support from the Research Facilities Improvement Program, Grant number C06 RR-RR016511, from the National Center for Research Resources, National Institutes of Health.

Submitted for publication September 30, 2010; revised February 14 and 25, 2011; accepted February 27, 2011.

Disclosure: **M. Michaelides**, None; **J. Rha**, None; **E.W. Dees**, None; **R.C. Baraas**, None; **M.L. Wagner-Schuman**, None; **J.D. Mollon**, None; **A.M. Dubis**, None; **M.K.G. Andersen**, None; **T. Rosenberg**, None; **M. Larsen**, None; **A.T. Moore**, None; **J. Carroll**, None

Presented in part at the annual meeting of the Association for Research in Vision and Ophthalmology, Fort Lauderdale, Florida, April 2010.

*Each of the following is a corresponding author: Michel Michaelides, UCL Institute of Ophthalmology, 11-43 Bath Street, London, EC1V 9EL, UK; michel.michaelides@ucl.ac.uk.

Joseph Carroll, Department of Ophthalmology, Medical College of Wisconsin, Milwaukee, WI, 53226; jcarroll@mcw.edu.

trichromacy.[2] Evidence in support of this hypothesis has been obtained by Keunen et al.,[4] who observed reduced foveal cone photopigment density with a normal time constant of photopigment regeneration in all four tested patients. In the majority of patients who have been studied in detail to date, color vision tests have revealed either completely normal color vision or slightly elevated discrimination thresholds.[2–9] Slightly elevated discrimination thresholds are compatible with a reduction in cone number. Further evidence is available from anomaloscopy, which in one study was undertaken in all six subjects and revealed matching ranges within normal limits,[6] indicating the presence of long- and middle-wave cones of normal spectral sensitivity at the macula; while the absence of pseudoprotanomaly suggests that photopigment is present at normal optical densities in individual cone photoreceptors. These findings when taken together support the hypothesis of a reduced number of foveal cones with otherwise normal functioning residual cones.

In the majority of patients identified to date, no clear underlying molecular genetic basis has been identified. There is some evidence suggesting that in limited cases hypomorphic mutations in genes associated with the recessive cone dysfunction syndrome, achromatopsia, may be involved (*GNAT2*, *CNGA3*, *CNGB3,* and *PDE6C*).[7,9,10] However, some of these cases arguably have features more in keeping with incomplete achromatopsia per se, rather than OT. In addition, only single heterozygous missense variants have been identified in other subjects, thereby rendering their significance currently uncertain.[7,10]

Recently, optical coherence tomography (OCT) has been used in an attempt to probe the structural basis of OT. Andersen et al.[7] obtained images in four individuals and found that retinal thickness was normal at the fovea but mildly reduced in the parafoveal and perifoveal regions. A general reduction in retinal layer reflectivity was also observed, with no other notable abnormalities in the appearance of the different layers.[7] Vincent et al.[9] examined a single case of OT and also reported qualitatively normal OCT images. It thus remains unclear whether the reduced cone function in OT is due to a reduced number of cones or whether the cones are present but not functioning normally.

In this study we used adaptive optics retinal imaging to directly assess the integrity of the cone photoreceptor mosaic in four patients with OT. In addition, spectral domain OCT was used to assess the integrity of the intraretinal layers, including quantitative analysis of the photoreceptor inner and outer segment lengths. While the phenotypic heterogeneity described extends to the cellular level, our findings demonstrate an important role for high-resolution imaging of photoreceptor structure in more accurate classification of the phenotype in OT and other related photoreceptor disorders.

Patients and Methods

Patients

This study followed the tenets of the Declaration of Helsinki (1983 Revision) and was approved by the local ethics committees. Informed consent was obtained from all subjects after the nature and possible consequences of the study were explained. We examined four patients, whose clinical phenotype has been previously described in detail.[6,7] JC-160 and JC-161 (brothers) are patients 1 and 2, respectively, in the report by Michaelides et al.[6] JC-071 is patient A and RB-1002 is patient E in the publication by Andersen et al.[7] For reference, a brief summary of the clinical findings is shown in Table 1.

Methods

Adaptive Optics Retinal Imaging. Images of the photoreceptor mosaic were obtained using one of two identical adaptive optics (AO) fundus cameras (housed at the Medical College of Wisconsin and Buskerud University College) employing a previously described

Table 1. Summary of Clinical Findings

	JC-160	JC-161	JC-071	RB-1002
Sex	Male	Male	Male	Female
Age, y	15	13	47	26
Nystagmus	None	None	Yes	None (history of mild congenital nystagmus)
BCVA				
OD	20/30	20/40	20/50	20/30
OS	20/30	20/40	20/70	20/30
Refractive error				
OD	+0.75/−2.75 × 10	plano/−1.50 × 25	+1.00	+5.50/−1.25 × 50
OS	+0.50/−2.25 × 175	+0.75/−1.50 × 180	+0.50	+5.25/−1.00 × 135
Axial length, mm				
OD	24.22	25.08	22.34	21.18
OS	24.14	25.22	22.71	21.23
Photopic single-flash*	Absent	Absent	54.0	4.56
Photopic flicker response†	Absent	Absent	51.7	Absent
Rayleigh match‡	~39–44	~39–44	41–41	38–43
D-15	No errors	No errors	No errors	No errors
Ishihara plates	No errors	No errors	No errors	3 errors
Cambridge Color Test§	187 (P) 136 (D) 399 (T)	302 (P) 230 (D) 171 (T)	Not done	109 (P) 101 (D) 813 (T)
Genetic summary	No mutations found‖	No mutations found‖	c1208G>A p.Arg403Gln heterozygous *CNGB3*¶	No mutations found¶

Patients JC-160 and JC-161 are brothers. BCVA, best-corrected visual acuity.

* Median amplitude (5–95th percentile) = 136 mV (76–201).

† Median amplitude (5–95th percentile) = 101 mV (61–154).

‡ All match ranges and midpoints are within normative values for the respective devices on which they were measured.

§ Normal trivector values for protan (P), deutan (D), and tritan (T) axes are 69.3, 82.4, and 113.4.[11]

‖ Genes examined: CNGA3, CNGB3, RGS9, R9AP, OPN1MW/OPN1LW array.

¶ Genes examined: CNGA3, CNGB3, GNAT2, KCNV2, PDE6C, OPN1MW/OPN1LW array.

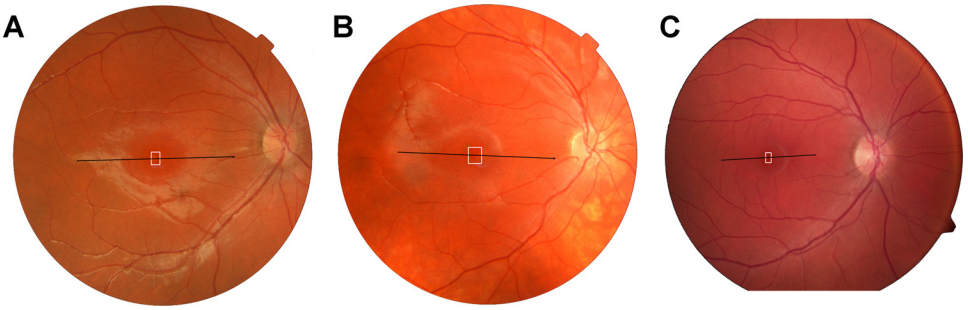

FIGURE 1. Fundus images from JC-160 (**A**), JC-161 (**B**), and RB-1002 (**C**) showing registration of the OCT scans (Fig. 6) and AO montages (Fig. 3).

protocol.[12] In brief, in a continuous closed-loop fashion, the eye's monochromatic aberrations were measured over a 6.4 mm pupil with a Shack-Hartmann wavefront sensor and corrected for with a 52-channel deformable mirror (Imagine Eyes, Orsay, France). Once a wavefront correction was obtained, a retinal image was acquired by illuminating the retina with a 1.8° diameter, 500 ms flash of light controlled by a mechanical shutter. A back-illuminated, scientific-grade, 12-bit charge-coupled device (CCD) (Cam1M100-SFT, Sarnoff Corporation, Princeton, NJ) captured images of the retina; acquisition was triggered electronically via a computer-controlled D/A module (DT9854; DataTranslation, Marlboro, MA) and associated driver circuit. This CCD is a frame transfer camera with a light-sensitive area of 1024 × 512 pixels. During each 500 msec shutter-controlled exposure, continuously triggered images of the retina were collected at a frame rate of 167 Hz with a 6 msec exposure.

Images were collected at different locations across the central fovea. After background correction, all images were registered using a custom software program (MATLAB; MathWorks, Natick, MA) and averaged. The location of individual cones was measured using an automated algorithm, which also allowed manual addition or subtraction of cones missed or selected in error by the algorithm.[13,14]

Spectral Domain Optical Coherence Tomography. For all subjects, volumetric images of the macula were obtained using high-definition optical coherence tomography (Cirrus HD-OCT; Carl Zeiss Meditec, Dublin, CA). Volumes were nominally 6 mm × 6 mm and consisted of 128 B scans (512 A scans/B scan). Retinal thickness was calculated using the built-in macular analysis software (software version 5.0), which is automatically determined by measuring the difference between the inner limiting membrane (ILM) and retinal pigment epithelium (RPE) boundaries. In three subjects (JC-071, JC-160, JC-161), high-resolution spectral domain optical coherence tomography (SD-OCT) images of the macula were acquired (Bioptigen, Research Triangle Park, NC). High-density line scans (1000 A scans/B scan, 100 repeated B scans) were acquired through the foveal center. Line scans were registered and averaged to reduce speckle noise in the image as previously described.[15] Volumetric images were also acquired (1000 A scans/B scan, 100 B scans/volume) to aid in aligning the line scan to the fundus image (Fig. 1). In the fourth subject (RB-1002), high-resolution SD-OCT images of the macula were obtained using another SD-OCT system (Spectralis; Heidelberg Engineering, Heidelberg, Germany). The lateral scale of all OCT data sets was corrected for interindividual differences in axial length (Zeiss IOL Master; Carl Zeiss Meditech, Dublin, CA).

Foveal pit morphology was assessed based on a previously published algorithm (MATLAB; MathWorks, Natick, MA).[16,17] Longitudinal reflectivity profiles (LRPs) were obtained as previously described.[18] Using the LRP analysis, we assessed the inner segment (IS) and outer segment (OS) length at the fovea. IS length was defined as the peak-to-peak distance from the external limiting membrane (ELM) to the IS/OS, while OS length was defined as the peak-to-peak distance from the IS/OS to the first peak in the RPE complex (RPE1).[18] We have shown previously that these definitions result in IS and OS measurements that match those obtained from histology.[18,19] For SD-OCT layer analysis, we analyzed a normative database collected at the Medical College of Wisconsin. This database has been previously published in part[13,18] and consists of 167 individuals (72 male, 95 female), with an average age of 32.6 ± 15.4 years (range 7 to 60 years).

RESULTS

Adaptive Optics Imaging

Reduced Cone Density in Oligocone Trichromacy. The two brothers (JC-160 and JC-161) and adult female (RB-1002) had significantly disrupted cone mosaics (Fig. 2). The cone density measured at ~1° temporal to the fovea was markedly reduced in all three subjects: 11,775 cones/mm^2 (JC-160), 25,225 cones/mm^2 (JC-161), and 14,848 cones/mm^2 (RB-1002) (Fig. 2). Normal cone density at this location has been shown previously to be 49,555 cones/mm^2 (SD ± 8707 cones/mm^2).[13] For reference, a normal age-matched retina is shown in Figure 2A, having a cone density of 41,850 cones/mm^2. No

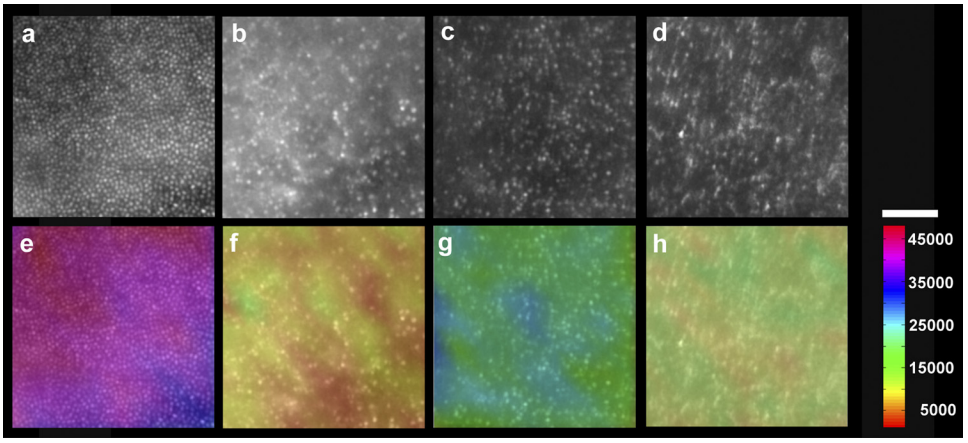

FIGURE 2. Images of the cone photoreceptor mosaic at ~1° temporal to the fovea, JC-160 (**B**), JC-161 (**C**), and RB-1002 (**D**) compared with an age-matched normal (**A**). All three subjects have dramatically disrupted mosaics. (**E–H**) Cone density is indicated by a color scale overlaid onto the respective mosaic images. The cone density in these panels was 41,850 cones/mm^2 (**E**, normal), 11,775 cones/mm^2 (**F**, JC-160), 25,225 cones/mm^2 (**G**, JC-161), and 14,848 cones/mm^2 (**H**, RB-1002). Scale bar, 50 μm.

obvious cone structure could be seen outside the central fovea in either brother or the female patient, with the imaged locations having few (if any) waveguiding cones.

Altered Cone Density Topography in Oligocone Trichromacy. The averaged images from different locations around the central fovea were stitched together to produce a larger montage for each of the two brothers and adult female (Fig. 3). Normal peak foveal cone density is 180,000 cones/mm^2.[20] The peak cone density measured in the normal retina shown in Figure 3A was 88,320 cones/mm^2, measured at ~0.25° (it was not possible to resolve the cones at the very center of the fovea due to an even higher density). In both brothers and the adult female, the cone mosaic was found to be discontiguous and of dramatically reduced density: JC-160 (peak density = 32,143 cones/mm^2), JC-161 (peak density = 29,281 cones/mm^2), and RB-1002 (peak density = 27,143 cones/mm^2). In addition, cone density was relatively uniform, in stark contrast to the rapidly changing density profile observed in normal eyes at this retinal location (Fig. 3A). These findings indicate that, in these three patients, both cone density and cone distribution are significantly disrupted.

Normal Cone Density in Oligocone Trichromacy. It is noteworthy that despite JC-071 having marked nystagmus, images of the cone mosaic could be acquired owing to the high-speed nature of the AO camera used. However, because of the nystagmus, we were not able to accurately place these images with a high degree of certainty within the context of the fundus image. As such, the estimates of cone density in these images cannot be assigned to a specific retinal location. Nevertheless, it is clear that the cone density was variable across the central retina in this patient, in direct contrast to the other three patients (Fig. 4). Cone density ranged from 18,491 cones/mm^2 to 57,779 cones/mm^2 (Fig. 4). In addition, also unlike JC-160, JC-161, and RB-1002, the cone mosaic was contiguously packed at all imaged locations (Fig. 4). These images fail to reveal any structural basis for the cone dysfunction observed in JC-071.

Spectral Domain Optical Coherence Tomography

SD-OCT images were obtained in all four patients (Figs. 5, 6, and 7). Retinal thickness was generally reduced in all four patients, though to a lesser extent in JC-071 and RB-1002 (Fig. 5). The

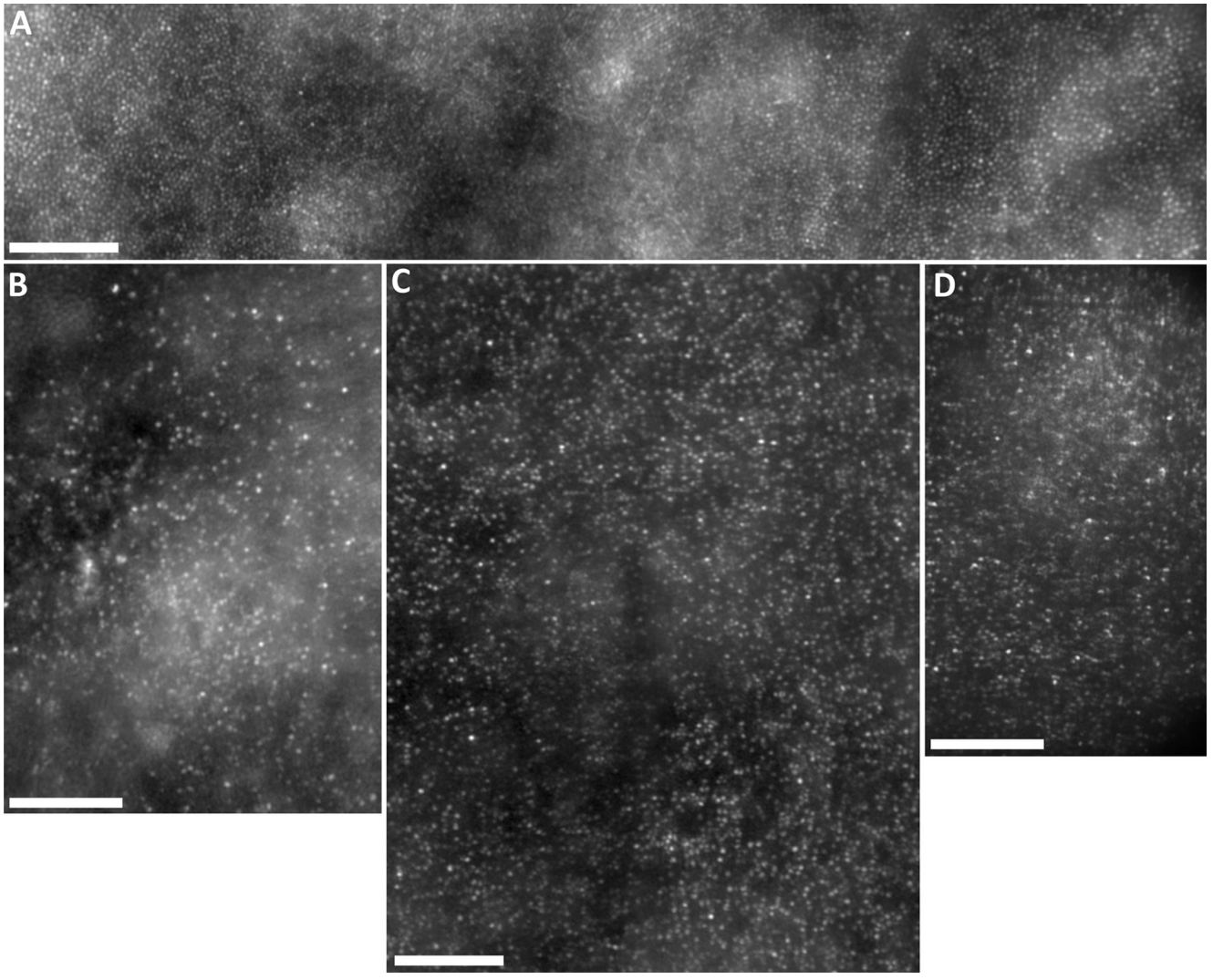

FIGURE 3. Adaptive optics montages of the foveal cone mosaic. (**A**) Normal cone mosaic with foveal center located near the center of the image. Peak cone density measured in this image (~0.25° away from the foveal center) was 88,320 cones/mm^2. (**B**) Foveal montage from JC-160; peak cone density within the montage was 32,143 cones/mm^2. (**C**) Foveal montage from JC-161; peak cone density within the montage was 29,281 cones/mm^2. (**D**) Foveal montage from RB-1002; peak cone density within the image was 27,143 cones/mm^2. Scale bar, 100 μm in all four panels.

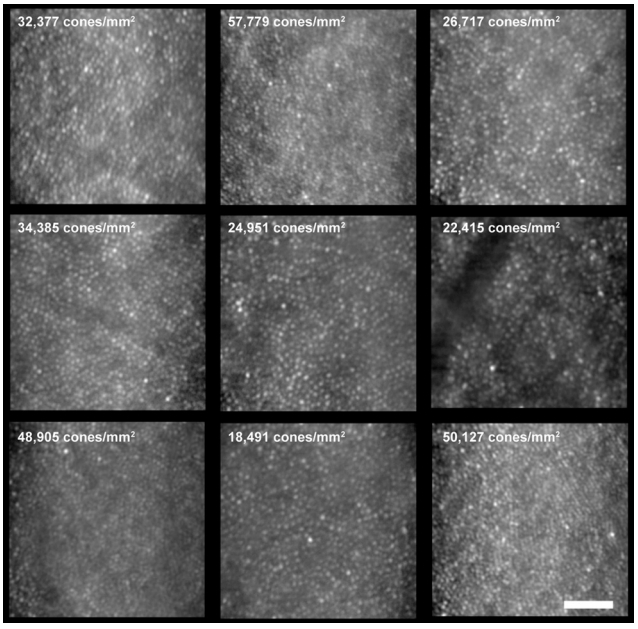

FIGURE 4. Images of the macular cone photoreceptor mosaic of patient JC-071 at nine locations. The cone density was variable across the central retina, in contrast to the two brothers (JC-160 and JC-161) and RB-1002. Cone density ranged from 18,491 cones/mm^2 to 57,779 cones/mm^2. In addition, also unlike the two brothers and RB-1002, the cone mosaic was continuously packed at all imaged locations. Scale bar, 50 μm.

relatively increased retinal thickness in the central subfield of JC-071 appears to be a result of a shallower foveal pit, with foveal pit depth being >3 standard deviations below the mean foveal pit depth observed in Caucasian subjects.[17] This shallowing may be related to the bilateral epiretinal membranes observed on imaging. Despite the abnormal foveal morphology and significant retinal thinning in many of the ETDRS segments for JC-071, all retinal layers were present and continuous (Figs. 6 and 7). In direct contrast, in the two brothers (JC-160 and JC-161) and female patient (RB-1002), retinal thickness was reduced (Fig. 5), and the outer segment/retinal pigment epithelium layer (RPE1) was absent in the periphery and mottled at the fovea (Figs. 6 and 7). In addition, in these three patients, the junction between the inner and outer segments of the cone photoreceptors was disrupted in the peripheral macula, showing reduced reflectivity relative to the foveal IS/OS junction (Fig. 6). As the IS/OS junction has been shown to have wave-guide properties consistent with the classical Stiles-Crawford effect,[21] the diminished intensity of the IS/OS observed here is in keeping with our observation that no obvious cone structure could be seen outside the central fovea in either brother or the female patient using AO imaging.

Using an LRP analysis, all four patients had normal IS lengths; however, JC-160, JC-161, and RB-1002 had significantly reduced OS lengths (Fig. 7). The apparent thinning of the OS layer could be due to the reduced number of wave-guiding cones at this location and/or a true reduction in OS length. For segmentation analysis, we defined the ILM, outer plexiform layer (OPL), ELM, and RPE2 layers, to calculate total retinal thickness (ILM-RPE2), inner retinal thickness (ILM-OPL), and outer nuclear layer (ONL) thickness (OPL-ELM) (Fig. 8). Consistent with the topographical thickness maps in Figure 5, we observed a marked reduction in total retinal thickness in the two brothers and female subject and a significant thinning of the nasal retina in JC-071 (Fig. 8). Importantly, central retinal thickness was preserved in JC-071, but reduced in JC-160, JC-161, and RB-1002. Further examination showed that the two brothers and female subject had a reduced ONL thickness (Fig. 8B) but normal inner retinal thickness (Fig. 8C). Thus the overall reduction in retinal thickness can be attributed to both reduced ONL thickness and reduced OS length in these individuals. However, in marked contrast to these three patients, JC-071 had relative preservation of central ONL thickness and significant thinning of the inner retina near the optic disc (Fig. 8B and 8C).

DISCUSSION

In this study we have probed the underlying structural basis of OT in an attempt to shed light on the pathogenesis and phenotypic variability reported in the disorder. In three patients in our series, the uniform reduction in cone density in association with a reduced ONL thickness is consistent with the hypothesis that OT is characterized by a reduced number of cones. The fact that these patients retain near-normal trichromatic color vision indicates that the remaining cones visible on AO imaging are indeed functional.

However, in the remaining unrelated male subject, both cone density and cone distribution appeared unperturbed, suggesting that, unlike the three other patients in our study, dysfunctional cones underlie the phenotype observed in this patient. Interestingly, a single heterozygous missense mutation in *CNGB3*, p.R403Q, has been previously identified in this patient[7], whereas no underlying mutations were identified in previously described candidate genes in the other three patients (Table 1). Mutations in *CNGB3*, the gene coding for the β-subunit of cone photoreceptor cGMP-gated cation channels, are commonly associated with achromatopsia.[1] However, to date, this particular variant has been identified only in progressive cone dystrophy (PCD), both as a compound heterozygous mutation in association with

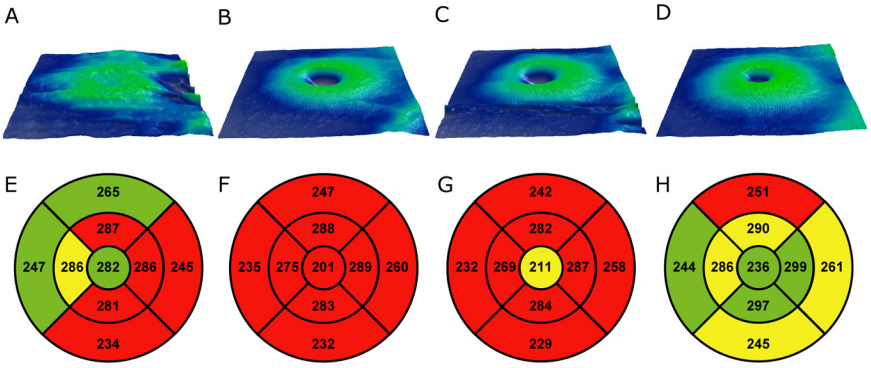

FIGURE 5. Topographical retinal thickness maps (Cirrus) for all four subjects. (**A**, **E**) JC-071; (**B**, **F**) JC-160; (**C**, **G**) JC-161; (**D**, **H**) RB-1002. ETDRS grids show that retinal thickness was generally reduced in all four patients, though to a lesser extent in JC-071 and RB-1002. The grids for the two brothers were obtained by modifying the birth date to allow comparison to the Cirrus database, which is for 18 years and over.

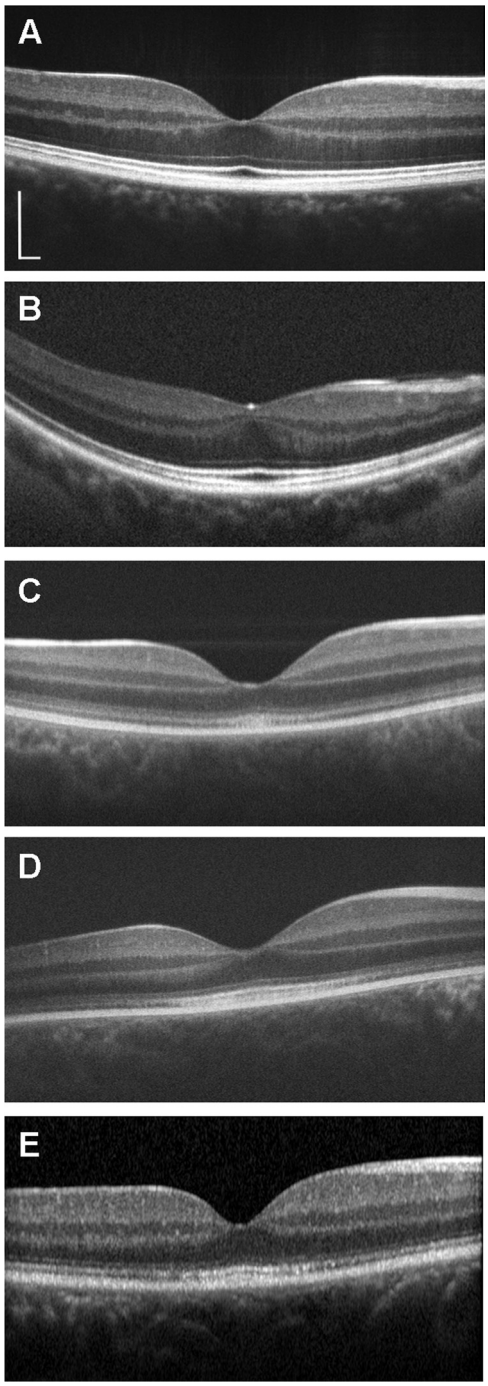

FIGURE 6. SD-OCT images (horizontal line scans) of patients JC-071 (**B**), JC-160 (**C**), JC-161 (**D**), and RB-1002 (**E**). A horizontal line scan of a normal control is shown for comparison (**A**). (**A–D**) Bioptigen SD-OCT; (**E**) Heidelberg Spectralis. The foveal pit is markedly shallower than normal in JC-071, whose retinal thickness was also reduced, although all retinal layers can be identified and appear to be continuous. In contrast, in JC-160, JC-161, and RB-1002, the OS/RPE layer is absent in the periphery and mottled at the fovea. The junction between the IS and OS of the cone photoreceptors is also disrupted in the peripheral macula relative to the fovea. Scale bar, 200 μm (vertical and horizontal), with the horizontal scale calibrated on the basis of axial length differences.

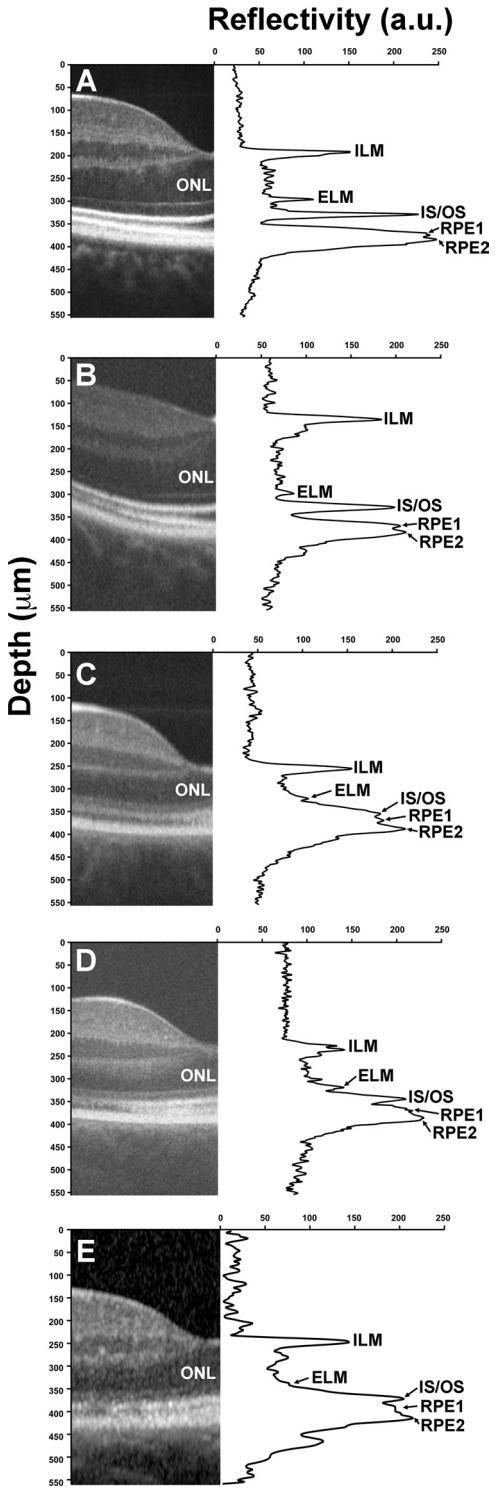

FIGURE 7. Assessing IS and OS length using longitudinal reflectivity profiles. (**A**) Normal control, (**B**) JC-071, (**C**) JC-160, (**D**) JC-161, and (**E**) RB-1002. IS length at the fovea was 32.19 μm (**A**), 29.89 μm (**B**), 32.19 μm (**C**), 27.89 μm (**D**), and 30.77 μm (**E**). Average IS length measured with the OCT technique used in our study is 31.13 $\pm$ 5.49 μm.[18] OS length at the fovea was 43.68 μm (**A**), 41.24 μm (**B**), 18.39 μm (**C**), 19.69 μm (**D**), and 19.23 μm (**E**). Average OS length measured with the OCT technique used in our study is 40.30 $\pm$ 4.47 μm.[18] To generate plots with a higher signal-to-noise ratio to enable easier peak detection, each plot represents an average of three neighboring LRPs centered at the foveal pit center.

p.Thr383fs, and in the homozygous state.[22–24] There has been no clinical evidence of progression in any of the subjects in our study. It would be of interest to image the

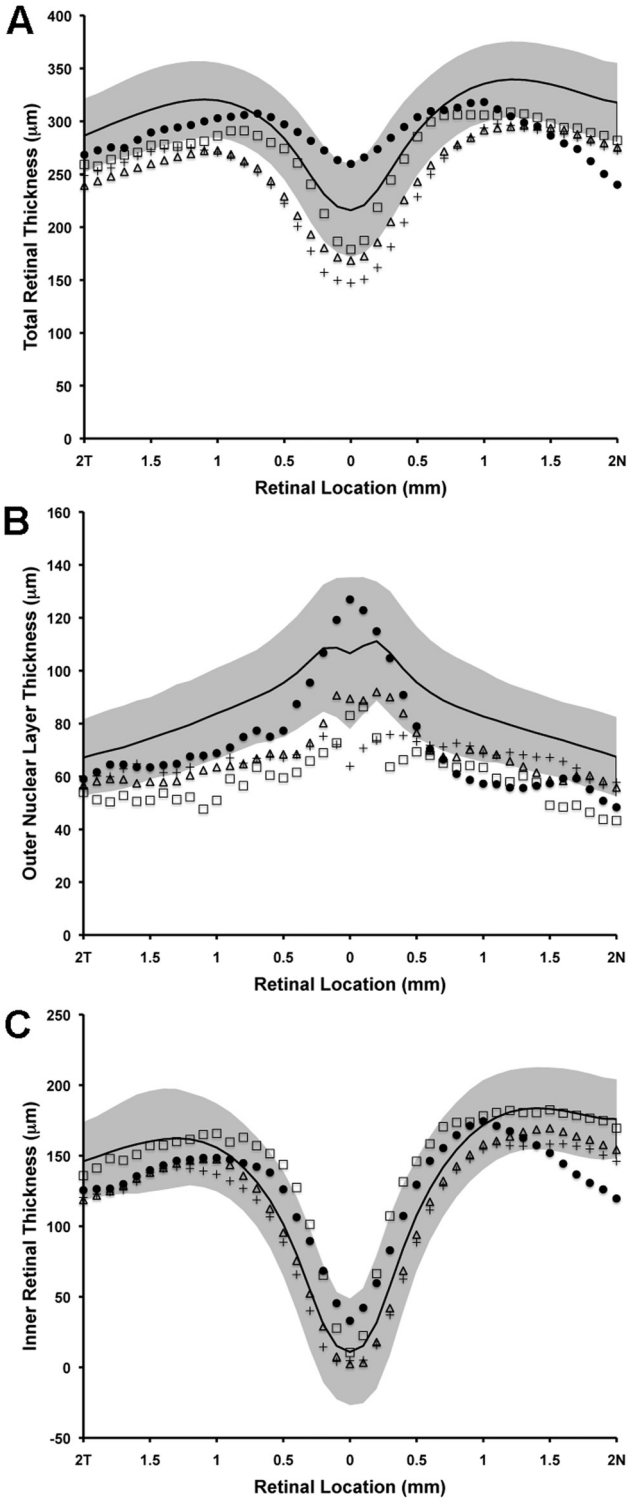

FIGURE 8. Retinal thickness analysis along the horizontal meridian. (**A**) Total retinal thickness, (**B**) outer nuclear layer thickness, (**C**) inner retinal thickness. *Solid black line* represents mean values for 167 normal controls, with *shaded region* representing ±2 standard deviations from the mean. JC-071, *filled circles*; JC-160, *crosses*; JC-161, *open triangles*; RB-1002, *open squares*.

mosaics of subjects with PCD who harbor this mutation, to help shed light on the pathologic mechanisms associated with this variant.

The identification of only single heterozygous missense variants in both the aforementioned subject and other patients from the same original OT molecular study,[7] including a novel heterozygous missense mutation in another phototransduction-related gene, *PDE6C*, renders their significance currently uncertain. Biallelic mutations in *PDE6C* have been reported as a rare cause of achromatopsia (complete and incomplete) and PCD.[25] These patients may represent carriers for mutant *CNGB3* and *PDE6C* alleles, respectively, with disease caused by mutations in another gene(s). It is also of interest that the mosaics seen in patients with achromatopsia are unlike those seen in the patients described herein.[26] Mutations in *RGS9* or *R9AP* have been reported in patients with a phenotype similar to OT, but such subjects have characteristic electrophysiological findings, which were not seen in our patients.[27] In addition, neither of the brothers in this study were found to harbor mutations in *RGS9* and *R9AP*.[27] Individuals with *RGS9*- or *R9AP*-associated retinopathy have cone mosaics that appear unlike those observed in the two brothers or female subject described in our study (Carroll, unpublished data). The identification of the major disease-causing genes in OT remains elusive, though it seems likely that the variable structural findings reflect underlying genetic heterogeneity.

The two groups of subjects described in our study (reduced cone number density versus normal cone mosaic) are difficult to discern on the basis of clinical phenotypic features alone. Quantitative high-resolution imaging may thereby prove to be an effective way of classifying subjects with cone dysfunction and normal color vision into OT and OT-like phenotypes, which may be useful in directing molecular genetic testing. Imaging further patients who have had a comprehensive candidate gene analysis will help to establish the validity of this proposal. Furthermore, the quantitative retinal imaging approach described herein may also help to shed light on the cellular basis of the phenotypic variability commonly observed in other inherited retinal disorders.

References

1. Michaelides M, Hunt DM, Moore AT. The cone dysfunction syndromes. *Br J Ophthalmol.* 2004;88:291–297.
2. van Lith GHM. General cone dysfunction without achromatopsia. In: Pearlman JT, ed. 10th ISCERG Symposium. *Doc Ophthalmol Proc Ser*. 1973;2:175–180.
3. Neuhann T, Krastel H, Jaeger W. Differential diagnosis of typical and atypical congenital achromatopsia. Analysis of a progressive foveal dystrophy and a nonprogressive oligo-cone trichromacy (general cone dysfunction without achromatopsia), both of which at first had been diagnosed as achromatopsia. *Graefes Arch Klin Exp Ophthalmol.* 1978;209:19–28.
4. Keunen JEE, De Brabandere SRS, Liem ATA. Foveal densitometry and color matching in oligocone trichromacy. In: Drum B, ed. *12th IRGCVD Symposium, Colour Vision Deficiencies XII.* Amsterdam: Kluwer Academic Publishers; 1995:203–210.
5. Ehlich P, Sadowski B, Zrenner E. Oligocone trichromasy, a rare form of incomplete achromatopsia. *Ophthalmologe.* 1997;94:801–806.
6. Michaelides M, Holder GE, Bradshaw K, et al. Oligocone trichromacy: a rare and unusual cone dysfunction syndrome. *Br J Ophthalmol.* 2004;88:497–500.
7. Andersen MK, Christoffersen NL, Sander B, et al. Oligocone trichromacy: clinical and molecular genetic investigations. *Invest Ophthalmol Vis Sci.* 2010;51:89–95.
8. Vedantham V, Kanungo S. Defective vision due to oligocone trichromacy in a young adult. *Indian J Ophthalmol.* 2006;54:289–290.
9. Vincent A, Wright T, Billingsley G, Westall C, Héon E. Oligocone trichromacy is part of the spectrum of CNGA3-related cone system disorders. *Ophthalmic Genet.* 2011;32:107–113.

10. Rosenberg T, Baumann B, Kohl S, et al. Variant phenotypes of incomplete achromatopsia in two cousins with GNAT2 gene mutations. *Invest Ophthalmol Vis Sci.* 2004;45:4256–4262.
11. Ventura DF, Silveira LCL, Rodrigues AR, et al. Preliminary norms for the Cambridge Colour Test. In: Mollon JD, Pokorny J, Knoblauch K, eds. *Normal & Defective Colour Vision*. Oxford: Oxford University Press;2003:331–339.
12. Rha J, Schroeder B, Godara P, Carroll J. Variable optical activation of human cone photoreceptors visualized using a short coherence light source. *Opt Lett.* 2009;34:3782–3784.
13. Carroll J, Baraas RC, Wagner-Schuman M, et al. Cone photoreceptor mosaic disruption associated with Cys203Arg mutation in the M-cone opsin. *Proc Natl Acad Sci U S A.* 2009;106:20948–20953.
14. Li KY, Roorda A. Automated identification of cone photoreceptors in adaptive optics retinal images. *J Opt Soc Am A Opt Image Sci Vis.* 2007;24:1358–1363.
15. Tanna H, Dubis AM, Ayub N, et al. Retinal imaging using commercial broadband optical coherence tomography. *Br J Ophthalmol.* 2010;94:372–376.
16. Dubis AM, McAllister JT, Carroll J. Reconstructing foveal pit morphology from optical coherence tomography imaging. *Br J Ophthalmol.* 2009;93:1223–1227.
17. Wagner-Schuman M, Dubis AM, Nordgren RN, et al. Race- and sex-related differences in retinal thickness and foveal pit morphology. *Invest Ophthalmol Vis Sci.* 2011;52:625–634.
18. McAllister JT, Dubis AM, Tait DM, et al. Arrested development: high-resolution imaging of foveal morphology in albinism. *Vision Res.* 2010;50:810–817.
19. Hoang QV, Linsenmeier RA, Chung CK, Curcio CA. Photoreceptor inner segments in monkey and human retina: mitochondrial density, optics, and regional variation. *Vis Neurosci.* 2002;19:395–407.
20. Curcio CA, Sloan KR, Kalina RE, Hendrickson AE. Human photoreceptor topography. *J Comp Neurol.* 1990;292:497–523.
21. Gao W, Cense B, Zhang Y, Jonnal RS, Miller DT. Measuring retinal contributions to the optical Stiles-Crawford effect with optical coherence tomography. *Opt Express.* 2008;16:6486–6501.
22. Michaelides M, Aligianis IA, Ainsworth JR, et al. Progressive cone dystrophy associated with mutation in CNGB3. *Invest Ophthalmol Vis Sci.* 2004;45:1975–1982.
23. Thiadens AA, Roosing S, Collin RW, et al. Comprehensive analysis of the achromatopsia genes CNGA3 and CNGB3 in progressive cone dystrophy. *Ophthalmology.* 2010;117:825–830.
24. Michaelides M, Hardcastle AJ, Hunt DM, Moore AT. Progressive cone and cone-rod dystrophies: phenotypes and underlying molecular genetic basis. *Surv Ophthalmol.* 2006;51:232–258.
25. Thiadens AA, den Hollander AI, Roosing S, et al. Homozygosity mapping reveals PDE6C mutations in patients with early-onset cone photoreceptor disorders. *Am J Hum Genet.* 2009;85:240–247.
26. Carroll J, Choi SS, Williams DR. In vivo imaging of the photoreceptor mosaic of a rod monochromat. *Vision Res.* 2008;48:2564–2568.
27. Michaelides M, Li Z, Rana NA, et al. Novel mutations and electrophysiologic findings in RGS9- and R9AP-associated retinal dysfunction (Bradyopsia). *Ophthalmology.* 2010;117:120–127.